

Spatiotemporal differentiation of the terrestrial gross primary production response to climate constraints in a dryland mountain ecosystem of northwestern China

Hao-jie Xu^{a,*}, Chuan-yan Zhao^a, Xin-ping Wang^b

^a State Key Laboratory of Grassland Agro-ecosystems, Key Laboratory of Grassland Livestock Industry Innovation, Ministry of Agriculture and Rural Affairs, Engineering Research Center of Grassland Industry, Ministry of Education, College of Pastoral Agriculture Science and Technology, Lanzhou University, Lanzhou, 730020, China

^b Shapotou Desert Research and Experiment Station, Northwest Institute of Eco-Environment and Resources, Chinese Academy of Sciences, Lanzhou, 730000, China

ARTICLE INFO

Keywords:

Carbon flux
Seasonal dynamics
Topography
Vegetation photosynthesis model
Statistical downscaling method

ABSTRACT

Monitoring seasonal and interannual variability in gross primary production (GPP) and attributing these changes to climate change across various ecosystems helps to predict the future climate-carbon cycle feedback. However, such studies are scarce in dryland mountain ecosystems, possibly because of high spatial heterogeneity in landscapes and terrain. To better understand how carbon fluxes of the dryland mountain ecosystem respond to meteorology, we identified the trend and driving mechanism related to GPP in the Qilian Mountains (QLMs) of northwestern China from 2000 to 2016 by adopting the vegetation photosynthesis model that incorporates satellite and meteorological data. Our results revealed contrasting GPP trends in the growing season (May–September) between 2000–2010 and 2010–2016. In the later period, widespread GPP reductions were found across almost the whole area, especially at the middle and end of the growing season. In the central part of the QLMs, GPP reductions were induced by warming hiatus in contrast to drought in the western and eastern parts. Responses of GPP to temperature, precipitation and solar radiation differed in seasons and biomes. The positive effect of rising temperature that increased GPP was dominant during the growing season. The interannual variability in GPP was positively related to precipitation in June and July, but was negatively related to precipitation in other months. A positive correlation between forest GPP and solar radiation occurred in all months but July. Desert GPP responded negatively to solar radiation in all months but September. Temperature and solar radiation accounted for most of the interannual variability in forest GPP. Temperature was the major climate constraints on the interannual variability in grassland GPP. Precipitation and solar radiation primarily controlled the interannual variability in desert GPP from July to September, while temperature became more limited than precipitation and solar radiation for desert GPP in May and June.

1. Introduction

Terrestrial gross primary productivity (GPP) is the photosynthetic carbon fixation by land plants per unit of time and surface area. GPP describes the initial inputs of carbon from the atmosphere to terrestrial ecosystems (Williams et al., 1997), and it serves as an indicator for ecosystem functions, especially production and regulation, which is essential for ensuring the well-being of people (de Groot et al., 2002). Quantifying the spatiotemporal variations of GPP and attributing these GPP changes to climate change at regional scales will be beneficial for ecosystem service assessment and deepen our understanding of the terrestrial carbon cycling (Heimann and Reichstein, 2008).

It remains a main challenge to simulate GPP at various scales but is

of priorities in carbon cycle studies. During the past decade, the eddy covariance (EC) technique has emerged as an important tool for calculating GPP from direct observations of carbon dioxide exchange at the canopy-atmosphere interface (Baldocchi, 2003). Nevertheless, such measurement is spatially limited due to the representativeness of flux sites in complex landscapes (Jung et al., 2009). Remote sensing techniques provide an alternative to evaluate the spatial-temporal patterns of GPP across multiple biomes at high spatial and temporal resolutions (Turner et al., 2006). The light use efficiency (LUE) model has been widely used to quantify GPP globally (Beer et al., 2010). It follows an algorithm of the photosynthetically active radiation (PAR), the fraction of absorbed PAR by the vegetation canopy ($fAPAR$), and the maximum LUE, down-regulated by environmental scalars, including air

* Corresponding author.

E-mail address: xuhaojie@lzu.edu.cn (H.-j. Xu).

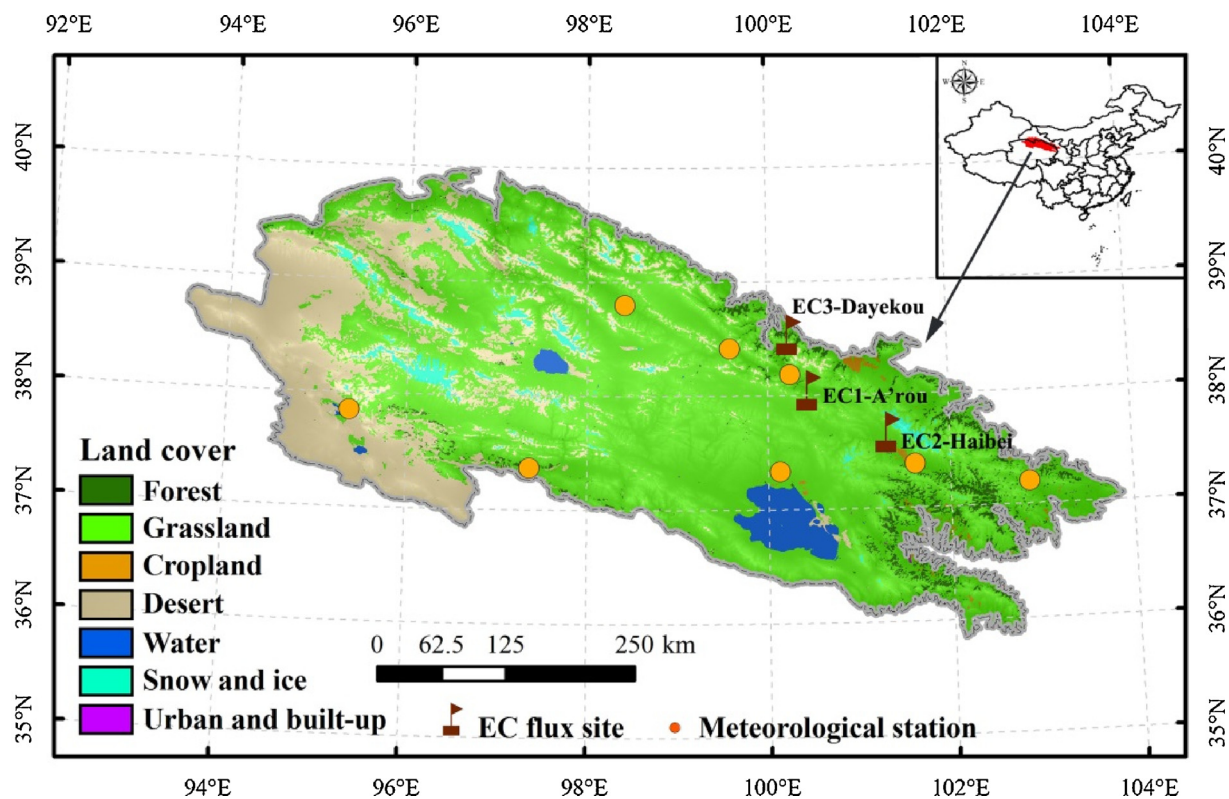


Fig. 1. The spatial distribution of meteorological stations, EC flux sites and land cover types in the QLMs. The base map is drawn, using the MODIS land cover type product (MCD12Q1) in 2016.

temperature, soil water content and vapor pressure deficit (Monteith, 1972). The uncertainty of LUE estimation among ecosystem types, meteorological forcings, along with confusing signals of *f*APAR caused by atmospheric interference, have a significant impact on the model accuracy (Jung et al., 2007).

Mountains are unique ecosystems that cover all latitudinally-controlled climate zones, and the vegetation in mountains is extremely vulnerable to climate mean and extremes (Diaz et al., 2003). The expected rate of climate warming in mountain areas during the 21st century might be two to three times greater than that in the 20th century (Nogués-Bravo et al., 2007). As a result, mountain systems are possibly the region most affected by future climate change. The main climate control on GPP is solar radiation, followed by temperature and precipitation, in tropical forests (Ichii et al., 2005). The GPP variability in temperate humid zones is primarily affected by temperature (Davi et al., 2006). In arid and semi-arid areas the relative importance of temperature on GPP variation decreases as water availability tightens the coupling between the meteorology and GPP variability (Nakano et al., 2008). It remains uncertain, however, to what extent temperature dominates GPP variability in dryland mountains, for the relationship between temperature and GPP varies in time and space, considering other climate constraints, such as precipitation and solar radiation (Saigusa et al., 2008).

The Qilian Mountains (QLMs) in northwestern China are the climatic divide between the East Asian monsoon and the westerlies. With the aid of mountain glaciers and precipitation, it functions as the water source to support irrigation agriculture in the Hexi Corridor—the famous Silk Road, and also as the ecological shelter to safeguard ecological viability in the northern Alxa Highland (Zhao et al., 2005). Since the 1960s, climate warming has led to an accelerated glacier retreat, alpine grassland degradation and biodiversity decline (Yao et al., 2016; Sun et al., 2018). Though the vegetation in the QLMs plays an important role in carbon sequestration, soil and water conservation (Sun et al., 2015; Wagner et al., 2015), few studies to date have examined the

magnitude and direction of GPP responses to climate change over large spatial scales (Fang et al., 2018). Applications of remote sensing to GPP modeling in the QLMs are precluded by limited meteorological data at high spatial resolutions, along with topographic and atmospheric effects on the quality of satellite images.

Previous studies show that the crucial climatic factors driving the interannual variation of GPP include temperature, precipitation and solar radiation (Nemani et al., 2003). It is not clear, however, their relative importance on the temporal variability of GPP and the climate-growth relationships across climates and ecosystems over the QLMs. For example, forest net primary production was positively correlated with downward shortwave radiation, but was negatively correlated with temperature and precipitation in the central QLMs from 2000 to 2012 (Yan et al., 2016). Over the past decade, increased precipitation and warming hiatus have promoted the growth of Qinghai spruce in the QLMs (Gao et al., 2018). Regarding an alpine meadow ecosystem in the QLMs, a positive correlation between GPP and temperature was observed, whereas there was a negative correlation between GPP and precipitation (Zhang et al., 2008). Conversely, soil moisture was a prime determinant of vegetation growth in an alpine steppe in the QLMs (Yao et al., 2016). Meanwhile, the natural vegetation shows seasonal variations of heat and water demand (Jia et al., 2016). Most previous studies are restricted to annual scale analyses of the GPP changes and their climate controls. However, little information is known about the difference in GPP variability at monthly and seasonal time scales (Wohlfahrt et al., 2008). These knowledge gaps highlight the imperative need for regional studies on the spatial variability and seasonal dynamics of GPP in the QLMs under global warming.

We hypothesize that the dependence of GPP on temperature may be changed at different growth stages of various vegetation types in the QLMs. Thus, we developed GPP products of the QLMs with a spatial and temporal resolution of 500 m and 8-day based on the Moderate Resolution Imaging Spectroradiometer (MODIS) satellite data and downscaled climatic data from the Climatic Research Unit (CRU) at the

University of East Anglia. The monthly GPP interannual variability and its relationships with temperature, precipitation and solar radiation were analyzed in each pixel over the period of 2000–2016. Our objectives were to investigate the trend and interannual variability in GPP in the QLMs, and determine the climate drivers of GPP dynamics varying in different seasons and biomes.

2. Materials and methods

2.1. Study area

This study focused on the Qilian Mountains (QLMs) located in the northeastern margin of the Tibetan Plateau. The QLMs span 35°50′–39°59′N in latitude and 93°31′–103°54′E in longitude, with a total area of approximately 2.0×10^5 km² (Fig. 1). It is bordered by the Hexi Corridor to the north, the Qaidam Basin to the south, the Altun Mountains to the west, and the Loess Plateau to the east. The elevation increases gradually from southeast to northwest, with the highest altitude reaching 5808 m. The QLMs are characterized by a plateau continental climate. The mean annual temperature for the period of 1981–2010 is -2.1°C, with the highest value of 10.2°C in July and the lowest of -15.5°C in January. The mean annual precipitation is 366 mm, 87.7% of which falls as rain between May and September. The mean annual solar radiation exceeds 7300 MJ m⁻². Major biome types in the QLMs involve grasslands, deserts, and forests, which account for 68.9%, 22.5% and 3.1% of the study area, respectively (Fig. 1). Temperature and precipitation change with elevation, leading to vertical vegetation zonation. It comprises warm deserts, desert steppes, alpine steppes, forests, alpine meadows, and alpine deserts as elevation rises. Forests are predominantly evergreen coniferous trees, dominated by *Picea crassifolia* and *Juniperus przewalskii*. Alpine grasslands are mainly composed of *Stipa* spp., *Kobresia myosuroides*, *Potentilla fruticosa* and *Caragana jubata*. Warm deserts include primarily *Salsola passerine*, *Slenderbranch Kalidium*, and *Ceratoides latens*. Alpine deserts consist mainly of high-altitude cushion-like and periglacial vegetation.

2.2. Data sources and preprocessing

2.2.1. Remote sensing products

The MODIS Terra MOD09A1 Version 6 land surface reflectance product with a spatial and temporal resolution of 500 m and 8-day from 2000 to 2016 was provided by the Land Processes Distributed Active Archive Center (LP DAAC, <https://lpdaac.usgs.gov/>). It has been corrected for atmospheric interference, such as gasses, aerosols, and Rayleigh scattering. The MODIS GPP product (MOD17A2H) at a spatial and temporal resolution of 500 m and 8-day, 2000–2016, was obtained from the Numerical Terradynamic Simulation Group (NTSG) at the University of Montana (<http://www.ntsg.umt.edu/>). Also, the MODIS land cover type product (MCD12Q1) at a 500 m resolution was obtained from the LP DAAC, 2001–2016. The plant functional types (PFT) classification scheme was employed. In the QLMs, forests comprise trees and shrubs. Grasslands are grasses. Croplands are cereal and broadleaf crops. Deserts are barren or sparsely vegetated lands, and are divided by elevation into two groups including warm deserts (2100–2500 m) and alpine deserts (> 3900 m). The digital elevation model (DEM) data with a spatial resolution of 500 m were derived from the NASA Shuttle Rader Topographic Mission (SRTM) website (<http://www.glcf.umd.edu/>).

2.2.2. Meteorological datasets

The CRU-NCEP Version 8 meteorological data over the period of 1961–2016, including daily maximum and mean air temperatures, daily precipitation and daily downward shortwave radiation, had a spatial resolution of $0.5^\circ \times 0.5^\circ$ and were downloaded from the below website: https://vesg.ipsl.upmc.fr/thredds/catalog/work/p529viov/cruncep/V8_1901_2016/catalog.htm. Daytime temperature was

defined as the average of daily maximum and mean temperatures. Temperature, precipitation and solar radiation data were averaged over an 8 day. The ground observation of monthly mean temperature and precipitation from 2000 to 2014 was collected from 8 meteorological stations over the QLMs (Fig.1), provided by the China Meteorological Data Service Center (<http://data.cma.cn/>). The station characteristics can be found in Table S1. The monthly climate layer of China for the period 1961–2000 was derived from the Chinese Ecosystem Research Network (CERN, <http://www.cern.org.cn/>). Such dataset include spatial interpolations of maximum and mean air temperatures, precipitation and solar radiation with a spatial resolution of 1 km. Based on 740 meteorological stations and a 1 km SRTM DEM, the monthly climate maps of China were drawn, by using a spatial interpolation tool implemented in geographic information systems. The raw CERN data were resampled at a 500 m resolution following a bilinear interpolation method implemented in the ArcMap Version 10.0 software. Observed monthly solar radiation was collected from the Gangcha (2000–2013) and Haibei (2000–2014) stations, available from the China Meteorological Data Service Center and the CERN, respectively (see Table S1 and Table S2 for more details).

2.2.3. EC-derived GPP data

Observed GPP at an 8-day interval was collected from 3 EC flux tower sites (Fig.1) and was acquired from previous researches (Zhang et al., 2008; Li et al., 2012; Wang et al., 2012). Details on the EC flux tower descriptions can be found in Table S2. CO₂ concentrations were measured using an open-path infrared gas analyzer (Li-7500, LiCor Inc., USA). The sampling frequency was 10 Hz. The CO₂ flux was calculated at 30 min interval and was processed with the despiking, coordinate rotation, angle of attack correction and WPL correction for all flux towers, of which the energy balance closure was > 80%, indicating the reliability of CO₂ flux measurements. GPP was calculated from the measured daytime net ecosystem exchange using EC and daytime ecosystem respiration. Nighttime net ecosystem exchange was hypothesized to be equal to ecosystem respiration. Daytime net ecosystem exchange was calculated based on the relationship established for nighttime net ecosystem exchange and meteorology.

2.3. Methods

2.3.1. Delta downscaling method

Meteorological stations are limited in number and show sparse spatial distribution in the QLMs, resulting in biased interpolations of climate variables and thus insufficient accuracy of simulated GPP. In this study, spatial patterns of the above-mentioned 8-day averaged climatic variables were obtained from 2000 to 2016 by employing the Delta downscaling process that incorporated terrain information and a bilinear interpolation technique (Mosier et al., 2014). It used the 500 m resolution CERN data as inputs to scale anomaly grids of the 0.5° resolution CRU-NCEP data.

For temperature downscaling, the process is as follows.

$$x_{i,j} - x_{a,j} = e_{i,j}; \quad e_{i,j} \rightarrow h_{i,j}; \quad h_{i,j} + X_{a,j} = y_{i,j} \quad (1)$$

where i and j are the annual and 8-day time-scales, respectively. a is the reference period. $x_{i,j}$ is the low resolution dataset. $X_{a,j}$ is the high resolution climatology. $e_{i,j}$ and $h_{i,j}$ are the anomaly at low and high spatial resolutions, respectively. $y_{i,j}$ is the downscaled data.

For precipitation and solar radiation downscaling, the anomaly is calculated as the ratio of the time series element and climatology.

$$\frac{x_{i,j}}{x_{a,j}} = e_{i,j}; \quad e_{i,j} \rightarrow h_{i,j}; \quad h_{i,j} \times X_{a,j} = y_{i,j} \quad (2)$$

In this study, i ranges from 2000 to 2016. j varies from 1, 9, 17, ..., 361. a is 1961–2000. $X_{a,j}$ has a fixed value every 8 day within a month. The downscaled monthly mean temperature, precipitation and

solar radiation data were validated against ground observations.

2.3.2. Vegetation photosynthesis model

The vegetation photosynthesis model (VPM) is designed on the basis of the conceptual partitioning of chlorophyll and non-photosynthetically active vegetation within a canopy, and computes GPP over the photosynthetically active period of vegetation (Xiao et al., 2004). The VPM-GPP has been successfully validated against the EC-GPP record across multiple biomes (Zhang et al., 2017). The VPM was driven by downscaled climatic data and MODIS satellite products to derive GPP at a 500 m resolution and an 8-day interval. The function used was:

$$GPP = PAR \times fAPAR_{chl} \times \varepsilon_g \quad (3)$$

where PAR accounts for 45% of the downward shortwave radiation ($MJ\ m^{-2}$). $fAPAR_{chl}$ is the fraction of absorbed PAR by leaf chlorophyll in the canopy. ε_g is the LUE ($g\ C\ MJ^{-1}$).

$fAPAR_{chl}$ is linearly related to the enhanced vegetation index (EVI), calculated by using red (620–670 nm) and near infrared (NIR, 841–876 nm) bands from the MOD09A1 product. The raw EVI data were processed with quality check, gap-filling and Savitzky-Golay filtering in the TIMESAT Version 3.0 software (Jönsson and Eklundh, 2004).

$$fAPAR_{chl} = (EVI - 0.1) \times 1.25 \quad (4)$$

$$EVI = 2.5 \times \frac{\rho_{NIR} - \rho_{Red}}{\rho_{NIR} + 2.4 \times \rho_{Red} + 1} \quad (5)$$

ε_g is regulated by the environmental scalar for temperature (T_{scalar}) and soil water content (W_{scalar}) from maximum LUE (ε^*).

$$\varepsilon_g = \varepsilon^* \times T_{scalar} \times W_{scalar} \quad (6)$$

$$T_{scalar} = \frac{(T - T_{max}) \times (T - T_{min})}{(T - T_{max}) \times (T - T_{min}) - (T - T_{opt})^2} \quad (7)$$

$$W_{scalar} = \frac{1 + LSWI}{1 + LSWI_{max}} \quad (8)$$

$$LSWI = \frac{\rho_{NIR} - \rho_{SWIR}}{\rho_{NIR} + \rho_{SWIR}} \quad (9)$$

where T_{max} , T_{min} , T and T_{opt} indicate the daytime maximum, minimum, mean and optimal air temperatures for vegetation productivity, respectively. LSWI is the land surface water index, estimated as the normalized difference between near infrared and shortwave infrared (SWIR, 1628–1652 nm) bands from the MOD09A1 product. $LSWI_{max}$ is the maximum LSWI during the growing season for individual vegetation pixels each year. The growing season of most vegetation lasted from May to September according to the phenological distribution, which was delineated from MODIS NDVI, using a threshold-based method for different vegetation groups (Zhou et al., 2016). T_{max} , T_{min} and T_{opt} were constant values for different biomes (Zhang et al., 2017). Based on multiple site level studies, ε^* had a constant value of 1.94, 1.72 and 1.24 $g\ C\ MJ^{-1}$ for forests, grasslands and deserts, respectively (Li et al., 2007, 2012; Wang et al., 2012). Critical parameters of the VPM can be found in Table S3. In the VPM, T , PAR, EVI and LSWI belong to the parameter varying across space and time.

The MCD12Q1 product provided biome type information for the VPM annually. The missing observation about the biome type in 2000 was derived from that in 2001. There were 46 raster layers of the VPM-GPP within one year, each of which represented GPP for an 8-day average. Monthly GPP was calculated as the sum of daily GPP ($g\ C\ m^{-2}$). The vegetated land was defined as mean annual GPP $> 1.0\ g\ C\ m^{-2}$, and the barren land and cropland was excluded. The variability of modeled GPP was validated against EC-GPP. VPM-GPP was also compared with MODIS GPP data in terms of interannual variations, due to

limited time series of EC-GPP.

2.3.3. Time trend analysis

The Mann–Kendall test was used to analyze the monthly GPP trend in each grid for the QLMs from 2000 to 2016. This method belongs to a non-parametric significance test, which detects monotonic trends in a time-varying variable and remains insensitive to abrupt changes (Mann, 1945). Positive values of the Mann–Kendall test (Z_s) indicate an increasing trend and vice versa. The values of ± 1.28 , ± 1.64 and ± 2.32 suggest 10%, 5% and 1% significant levels of the trend in the Mann–Kendall test. The magnitude of monthly GPP trends was calculated with the Sen's slope. It makes a reliable estimate of monotonic trends and has low sensitivity to outliers (Sen, 1968). The GPP trend was considered significant if the absolute value of Z_s was > 1.28 . The turning point of growing season GPP trend was determined by minimizing the residuals of piecewise linear fits, with the significance of turning point being tested by the t -test against the null hypothesis and the Akaike Information Criterion (ΔAIC), which offers a means for the selection between the simple linear regression and the two-part piecewise linear regression models (Xu et al., 2017).

2.3.4. Correlation analysis

The partial correlation coefficient of monthly GPP with temperature, precipitation and solar radiation was calculated in each grid. It assesses the relationships between two variables after eliminating the impact of other variables. t -tests were used to determine the significance level for the partial correlation coefficient. The values of ± 1.77 , ± 2.16 and ± 3.01 suggest 10%, 5% and 1% significant levels of the correlations in the t -test ($df = 13$). The P -value < 0.1 was considered significant.

2.3.5. Multivariable linear regression model

The multivariable linear regression model was adopted to simulate the GPP interannual variability with temperature, precipitation and solar radiation. Time series of the monthly GPP and the corresponding climatic factors was detrended in each grid. We then used the standard regression coefficient to determine the relative contribution of each climatic factor to the GPP interannual variability (Yao et al., 2018).

$$Y = b_0 + b_1 \times X_1 + \dots + b_i \times X_i + \mu \quad (10)$$

$$\text{Beta} = b_i \times \frac{\text{Std}(X_i)}{\text{Std}(Y)} \quad (11)$$

where b_0 is the constant value. b_i ($i \geq 1$) is the partial regression coefficient. μ is the random error. Beta is the standard regression coefficient. $\text{Std}(X_i)$ and $\text{Std}(Y)$ are the standard deviation of independent and dependent variables, respectively. The Beta of three climate variables was normalized to obtain RGB combination to determine the climate drivers of GPP dynamics.

2.3.6. Statistical analysis

Using the MATLAB R2014b, the Kruskal–Wallis test was used to assess for significance differences on continuous dependent variables by categorical independent variables ($\alpha = 0.05$). This method is a non-parametric version of classical one-way analysis of variance (ANOVA), and an extension of the Wilcoxon rank sum test to more than two groups (Kruskal and Wallis, 1952). The reason why the Kruskal–Wallis test was used was that the compared data were not always normally distributed and did not have variance homogeneity. Moreover, the root mean squared errors (RMSE) were used to quantify the agreement between observed and simulated values.

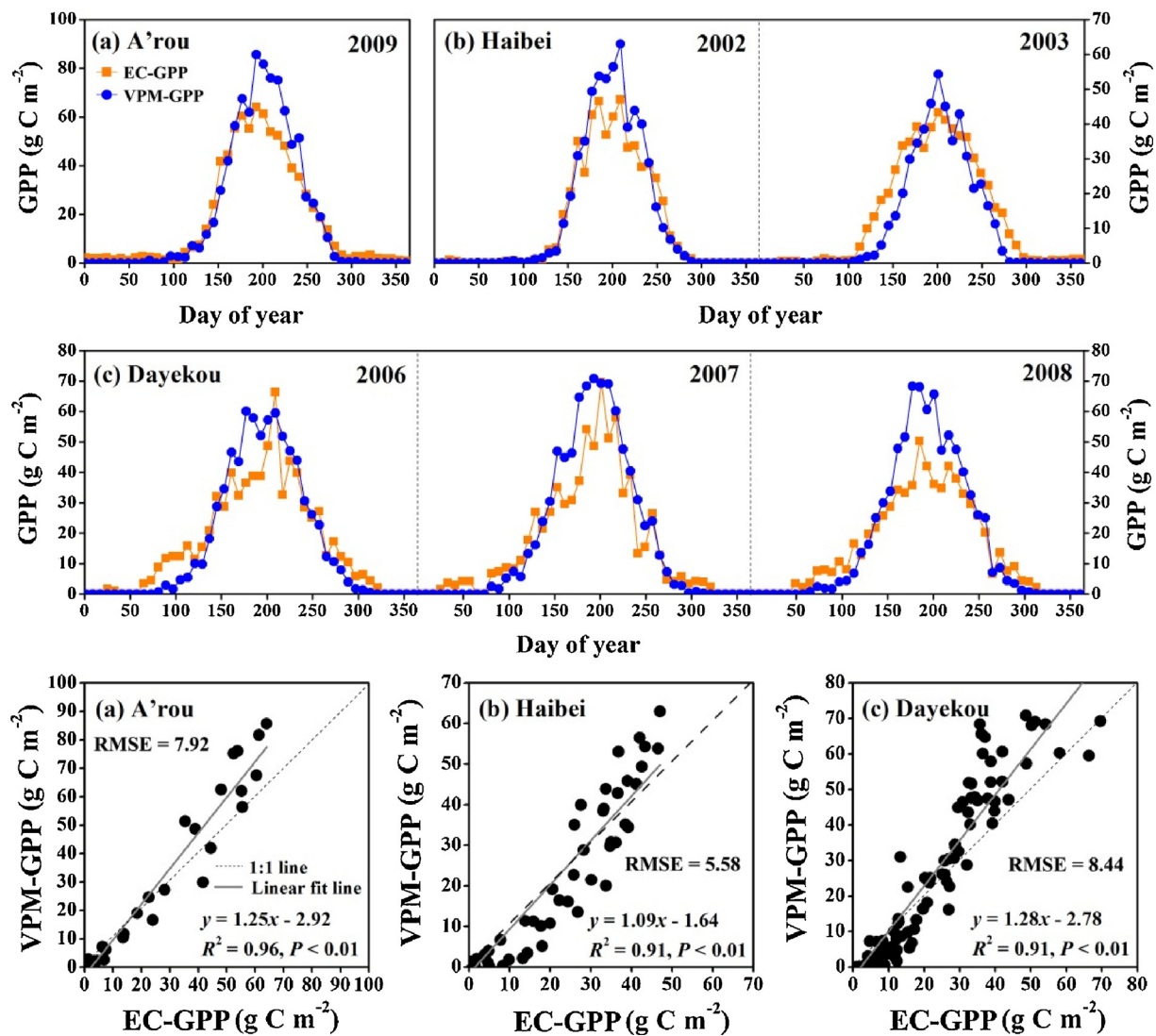


Fig. 2. The comparison of 8-day EC-derived GPP and VPM-simulated GPP at A'rou (a), Haibei (b) and Dayekou flux sites (c).

3. Results

3.1. Validation of simulated climate and GPP data

The regression analysis suggested that the Pearson correlation coefficient of downscaled and observed temperature was highest (0.98) in August but was lowest (0.89) in November (Fig.S1). The correlation between downscaled and observed precipitation ranged from 0.55 in December to 0.89 in September. The coefficient of determination was > 0.5 in all months but December (Fig.S2). The Pearson correlation coefficient of the predicted and observed values of solar radiation was > 0.95 (Fig.S3). The RMSE of monthly mean temperature varied from 0.6 to 1.8°C, with a mean of 1.1°C. The RMSE of monthly precipitation and solar radiation was 9.7 (1.3–23.7) mm and 43.3 (41.9–44.6) MJ m⁻², respectively.

The Pearson correlation coefficient of VPM-GPP and EC-GPP was 0.98, 0.95 and 0.95 at the A'rou, Haibei and Dayekou sites, respectively (Fig. 2). The corresponding RMSE of 8-day GPP reached 7.92 g C m⁻², 5.58 g C m⁻² and 8.44 g C m⁻². The differences between annual VPM-GPP and EC-GPP ranged from -19.3% to 13.8% in an alpine meadow and from 0.6% to 17.8% in an evergreen coniferous forest (Table 1). Compared with MODIS-GPP, VPM-GPP showed higher estimation in 70.7% of the vegetated lands of the QLMs, dominated by forests and grasslands (Fig.S4). For deserts, MODIS-GPP was higher than VPM-GPP

Table 1

Summary of calculated GPP from EC measurements and simulated GPP derived from the VPM at 3 flux sites (g C m⁻²).

| Flux site | Ecosystem type | Year | EC-derived data | | VPM-derived data | |
|-----------|-----------------------------|------|----------------------|-----------------------|-----------------------|--------|
| | | | GPP ₍₅₋₉₎ | GPP ₍₁₋₁₂₎ | GPP ₍₁₋₁₂₎ | RE |
| A'rou | Alpine meadow | 2009 | 733.8 | 803.9 | 874.5 | 8.8% |
| Haibei | Alpine meadow | 2002 | 492.8 | 503.9 | 573.3 | 13.8% |
| | | 2003 | 559.5 | 604.7 | 487.8 | -19.3% |
| Dayekou | Evergreen coniferous forest | 2006 | 621.7 | 750.0 | 754.2 | 0.6% |
| | | 2007 | 648.6 | 735.2 | 839.3 | 14.2% |
| | | 2008 | 572.0 | 678.5 | 799.0 | 17.8% |

GPP₍₅₋₉₎ and GPP₍₁₋₁₂₎ show the growing season and annual GPP, respectively. RE = [(GPP_{VPM} - GPP_{EC}) / GPP_{EC}] × 100%.

in most cases. Furthermore, MODIS-GPP underestimated EC-GPP by 16.1%–29.9% and 15.4%–35.3% in forests and grasslands, respectively. Annual VPM-GPP was positively correlated with annual MODIS-GPP in 92.5% of vegetated lands, 60.3% of which the relationship was significant ($P < 0.1$).

3.2. Changes in mean annual GPP across regions and biomes

The mean annual GPP for the period of 2000–2016 was 182.6 g C

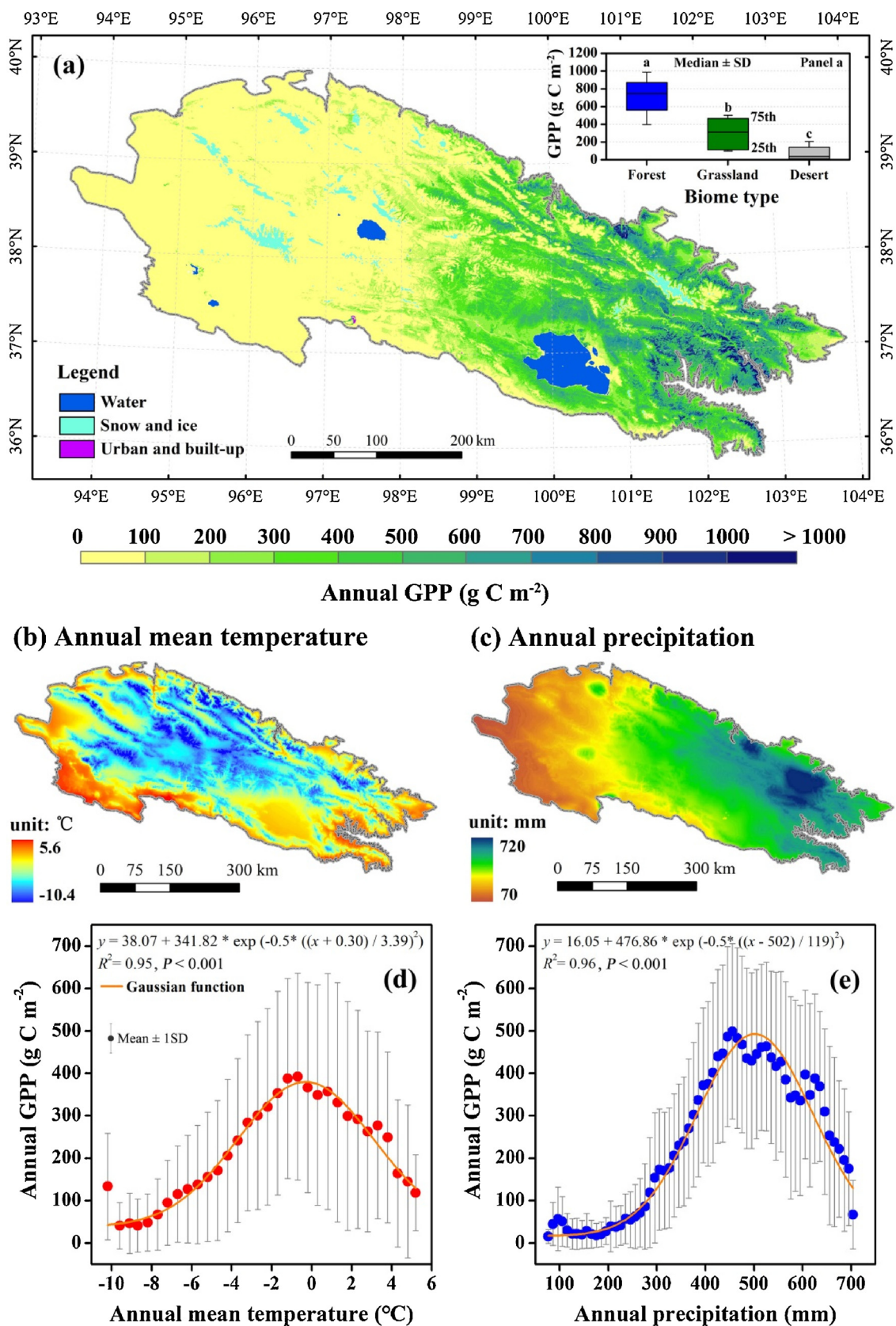


Fig. 3. The spatial distribution of mean annual GPP (a), temperature (b) and precipitation (c) over the period 2000–2016. Annual GPP varies with annual mean temperature (d) and annual precipitation (e). Different letters show significant differences in the insert graph.

m^{-2} in the QLMs, with the total GPP reaching 36.5 Tg C ($1 \text{ Tg} = 10^{12} \text{ g}$). High values of annual GPP were found in the eastern and central parts of the QLMs, which was in consistent with the spatial distribution of annual precipitation (Fig. 3a,c). In addition, annual GPP followed a biphasic trend with annual mean temperature and precipitation (Fig. 3d,e). That is, GPP increased with temperature when its value reached -0.3°C but decreased with temperature rises. Similarly, a two-stage pattern of GPP and precipitation was found when annual precipitation was approximately 500 mm . At the biome level, forests represented the largest annual GPP (Median \pm SD, $746 \pm 295 \text{ g C m}^{-2}$), followed by grasslands ($312 \pm 201 \text{ g C m}^{-2}$) and deserts ($32 \pm 152 \text{ g C m}^{-2}$) (Fig. 3a).

3.3. Interannual variations of monthly GPP

Only GPP dynamics and its relationships with climatic factors during the growing season were analyzed as monthly GPP was low during the non-growing season (Fig. 2). The two-part piecewise linear regression model indicated a turning point of growing season GPP trend in 2010 ($\Delta\text{AIC} = -2.46$). The total growing season GPP in the QLMs increased at a rate of $0.64 \text{ Tg C yr}^{-1}$ ($P < 0.1$) from 2000 to 2010 but then decreased at a rate of $-1.96 \text{ Tg C yr}^{-1}$ from 2010 to 2016 ($P < 0.05$) (Fig. 4). Meanwhile, such opposite trends between 2000–2010 and 2010–2016 were also found in growing season temperature, precipitation and solar radiation. Nevertheless, these trends were not statistically significant, except for an increasing trend in growing season precipitation for the period 2000–2010 (4.71 mm yr^{-1} , $P < 0.1$). The partial correlation coefficient (r) of GPP and precipitation was 0.49 ($P = 0.06$). Low correlations were found between GPP and temperature ($r = 0.30$, $P = 0.27$), followed by solar radiation ($r = -0.11$, $P = 0.69$). At monthly time scales, a significant increasing trend in GPP from 2000 to 2010 was detected in May, June, August and September (Table 2). The increasing rate was higher in June and August ($0.20 \text{ Tg C yr}^{-1}$) than September ($0.12 \text{ Tg C yr}^{-1}$) and May ($0.06 \text{ Tg C yr}^{-1}$). However, a significant decreasing trend in GPP from 2010 to 2016 was found in July, August and September. The decreasing rate was highest in July ($-0.90 \text{ Tg C yr}^{-1}$), followed by August ($-0.58 \text{ Tg C yr}^{-1}$) and September ($-0.26 \text{ Tg C yr}^{-1}$). Over the period of 2000–2016, only a significant positive correlation between GPP and temperature was observed in August ($r = 0.55$) and September ($r = 0.45$).

At the pixel scale, an increasing trend in monthly GPP was prevailing in most vegetated lands from 2000 to 2010 (Fig. 5). For this time period significant increases in GPP in June and July were found mainly

in the central and western parts of the QLMs ($P < 0.1$), dominated by grasslands and deserts. The area percentage of increasing GPP in June and July accounted for 40.1% and 26.9% of vegetated lands, respectively. In May, August and September, significant GPP increases were observed in the southern and eastern parts of the QLMs ($P < 0.1$), where most forests occurred. Percentage of the areas with increased GPP reached 22.2% , 32.6% and 35.5% , respectively. Most vegetated areas were dominated by a significant decreasing trend in monthly GPP from 2010 to 2016 ($P < 0.1$). Percentage of the areas with decreased GPP was larger in July (66.4%), August (47.8%) and September (40.2%) than in June (20.4%) and May (3.7%). In May and June, significant GPP decreases appeared mainly in the northwestern part of the Qinghai Lake ($P < 0.1$), including primarily alpine meadows. Widespread decreases in GPP emerged in the QLMs from July to August. In September, a decreasing trend in GPP was detected in the eastern and central parts of the QLMs, dominated by forests and grasslands.

At the biome level, the increasing rate of growing season GPP from 2000 to 2010 was highest in forests ($8.1 \text{ g C m}^{-2} \text{ yr}^{-1}$), followed by grasslands ($4.7 \text{ g C m}^{-2} \text{ yr}^{-1}$), but lowest in deserts ($1.5 \text{ g C m}^{-2} \text{ yr}^{-1}$) (Fig. 6). Similarly, the decreasing rate of growing season GPP during the period of 2010–2016 was higher in forests ($-19.1 \text{ g C m}^{-2} \text{ yr}^{-1}$) than grasslands ($-15.6 \text{ g C m}^{-2} \text{ yr}^{-1}$) and deserts ($-4.7 \text{ g C m}^{-2} \text{ yr}^{-1}$). Regarding forests and grasslands, the increasing rate of GPP within the growing season from 2000 to 2010 was higher in June and August. Such increasing rates were highest in deserts in July, followed by August. It was common that all biomes suffered larger GPP declines in July and August from 2010 to 2016, with the highest decreasing rate of GPP occurring in July.

3.4. Major climate drivers of monthly GPP interannual variability

During the growing season, 21.1% of vegetated regions presented a positive correlation between GPP and temperature ($P < 0.1$), particularly in the south of the Qinghai Lake and the central part of the QLMs (Fig. 7). Percentage of the areas with a negative correlation between GPP and temperature was low (2.4%), mostly in warm deserts (Table S4). Meanwhile, 20.6% of vegetated areas (20.6%) had a positive correlation between GPP and precipitation ($P < 0.1$) at low elevations of the QLMs, dominated by desert steppes and alpine steppes. A negative correlation between GPP and solar radiation emerged mainly at high altitudes (7.4% , $P < 0.1$). GPP was significantly correlated with climate variables in 44.5% of vegetated lands ($P < 0.1$).

From May to September, a significant positive correlation between

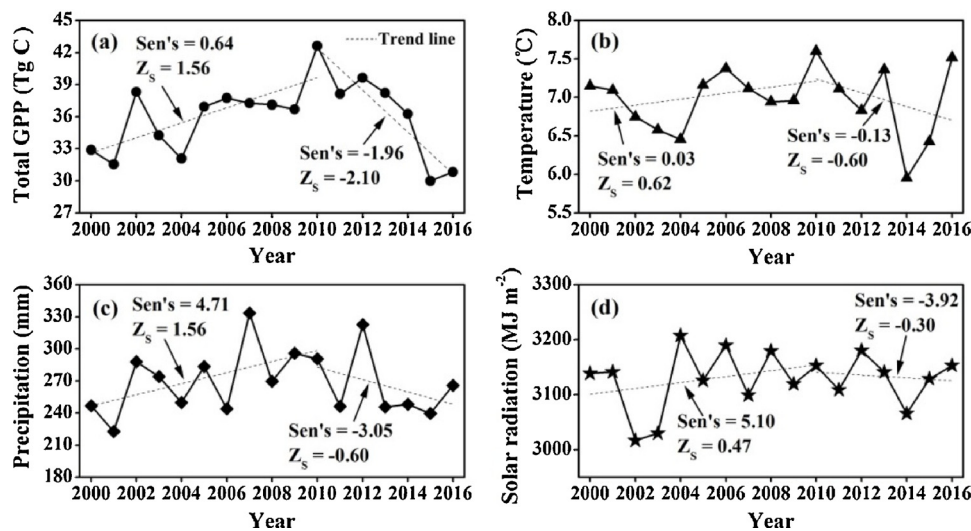


Fig. 4. The interannual variation of growing season GPP (a), growing season temperature (b), growing season precipitation (c) and growing season solar radiation (d), 2000–2016. Z_s shows values of the Mann–Kendall test.

Table 2

The Sen's slope of monthly GPP ($Tg\ C\ yr^{-1}$) in two different time periods (2000–2010 versus 2010–2016), and the correlation of GPP with temperature (r_T), precipitation (r_P), and solar radiation (r_S) at monthly time scales from 2000 to 2016.

| Month | Between 2000 and 2010 | | Between 2010 and 2016 | | Partial correlation coefficient | | |
|-----------|-----------------------|-------|-----------------------|-------|---------------------------------|-------|-------|
| | Sen's | Z_S | Sen's | Z_S | r_T | r_P | r_S |
| May | 0.06** | 1.87 | -0.01 | -0.30 | 0.33 | -0.08 | 0.19 |
| June | 0.20** | 1.71 | -0.23 | -1.20 | 0.30 | 0.26 | 0.12 |
| July | 0.07 | 0.62 | -0.90*** | -3.00 | 0.29 | 0.14 | -0.18 |
| August | 0.20 [†] | 1.56 | -0.58** | -1.80 | 0.55** | -0.24 | -0.09 |
| September | 0.12** | 2.18 | -0.26** | -1.80 | 0.45 [†] | 0.03 | 0.28 |

[†], ** and *** denote 10%, 5% and 1% significant levels. Z_S shows values of the Mann-Kendall test.

GPP and temperature was found in most vegetated lands ($P < 0.1$), while a significant negative correlation between GPP and temperature was found just in 2.9% of vegetated lands in September, mostly in some local regions of the western and central QLMs (Fig. 7). In May and June, 8.4% and 15.6% of vegetated lands showing a positive correlation between GPP and temperature emerged in the western part of the QLMs (Table S4). From July to September, such a positive correlation was observed mainly in the eastern and central portions. Percentage of the areas having a positive correlation between GPP and temperature reached highest in September (26.4%), followed by August (17.3%) and July (13.0%). Meanwhile, a significant positive correlation between GPP and precipitation ($P < 0.1$) in June was most obvious during the growing season, especially on the foot of the QLMs (12.9%). On the contrary, 6.3% and 7.7% of vegetated regions showed a negative correlation between GPP and precipitation in August and September, respectively, in the central QLMs. A significant positive correlation between GPP and solar radiation ($P < 0.1$) was detected in May, June and September, particularly in the eastern and central portions. The corresponding area reflecting positive GPP-solar radiation correlations occupied 10.5%, 7.0% and 9.3% of vegetated lands, respectively. Percentage of the vegetated lands with a significant correlation between GPP and climatic factors was highest in September (39.8%), followed by June (31%) and August (26.7%), but was lowest in July (23.1%) and May (22.9%).

Regarding all biome types, GPP was positively correlated with temperature from May to September (Fig. 8). Furthermore, GPP was positively related to precipitation in June and July but negatively correlated with precipitation in May, August and September. For most forests, a positive correlation between GPP and solar radiation was detected in all months but July. By contrast, GPP was negatively related to solar radiation in all months but September for most deserts. Grassland GPP was negatively correlated with solar radiation in July and August but positively correlated with solar radiation in other months. Generally, GPP was more positively correlated with temperature than precipitation and solar radiation in all biome types during the growing season (Fig. 8). An exception to this was that forest GPP was more positively related to precipitation than solar radiation and temperature in June. Such phenomenon also emerged in deserts, with a higher correlation between GPP and precipitation in July, and between GPP and solar radiation in September. With the same biome type, the partial correlation coefficient of GPP with climatic factors varied for different months (Fig. 8). For forests and grasslands, a positive correlation between GPP and temperature was highest in September. For deserts, the highest positive correlation between GPP and temperature appeared in June and August. GPP was more responsive to precipitation in June and July. As for the positive correlation between GPP and solar radiation, it was higher for forests in June and September. For grasslands such a higher correlation was found in May and September.

The major climate drivers of the interannual variability in GPP differed across time and space (Fig. 9). In the eastern part of the QLMs, temperature and solar radiation dominated the GPP interannual variability in most months during the growing season except for June,

when precipitation was a major climate driver. In comparison, the central portion of the QLMs was primarily affected by temperature from June to September but was affected by solar radiation in May. For the western part of QLMs, precipitation and solar radiation affected primarily the interannual variability in GPP from July to September. In May and June, temperature was the dominant climatic factor for GPP dynamics. Overall, during the growing season the responses of monthly GPP to climate variables in the QLMs were influenced primarily by temperature. Percentage of the temperature-dominated region ranged between 41% and 47.8%. In addition, percentage of the precipitation- and solar radiation-dominated area was largest in July (34.8%) and May (40.9%), respectively. Compared with May and June, precipitation outweighed solar radiation in driving the interannual variability in GPP from July to September.

4. Discussion

4.1. Evaluation of Delta downscaling method

Meteorological forcings are one of the important inputs for satellite-based simulation of GPP (Jung et al., 2007). Simplification of landscape complexity could cause GPP modeling to be considerably biased, particularly in mountainous regions (Sabtrafar et al., 2011), for the topography, such as elevation, slope and aspect, influences the distribution patterns of climate variables, including temperature, precipitation and solar radiation. Insufficient meteorological stations are distributed over the QLMs (Fig. 1), resulting in great uncertainty about the spatial interpolation result. To capture reliable meteorological data at fine spatial resolutions, we used a statistical downscaling technique. Although the simulated climatic data were slightly lower than the observation value, performance of the Delta downscaling method was satisfactory in predicting the distribution pattern of climatic factors over complex terrain (Fig.S1-3), for this method incorporated the topographical effect in the distribution of meteorology represented in high resolution input grids (Mosier et al., 2014). This study shows that the Delta downscaling method has a potential application for acquiring meteorological data at relatively high spatial resolutions in heterogeneous regions, which requires less computation time and limited field measurements. Nevertheless, the meteorological data currently considered are the results of a CRU-NCEP statistical downscaling, neglecting regional hydro-meteorological processes as its spatial resolution is approximately 500 km. Moreover, the high resolution climatology input (CERN data at a spatial resolution of 1 km) nested in a CRU-NCEP may contain systematic errors in simulating the distribution of meteorological variables when the terrain condition is highly heterogeneous (Wilby and Wigley, 1997).

4.2. Assessment of VPM-GPP

It is necessary to assess its performance when employing VPM-GPP to study the spatial and temporal variations of carbon fluxes over the QLMs. Our results indicated that VPM-GPP generally tended to

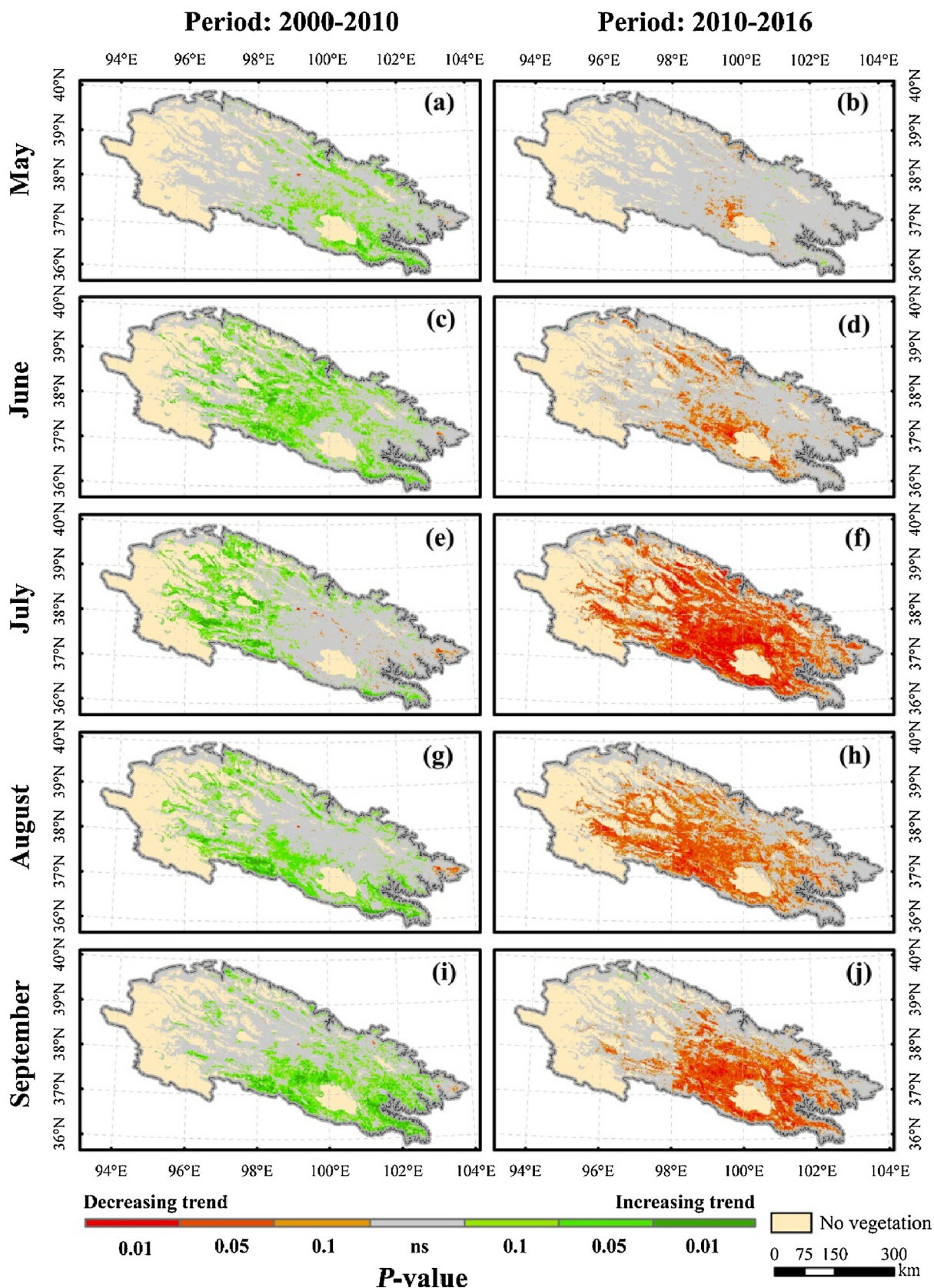


Fig. 5. The spatial distribution of monthly GPP trends for the period of 2000–2010 and 2010–2016, respectively.

overestimate 8 day and annual GPP when compared with calculated GPP from EC measurements for forests and grasslands (Fig. 2 and Table 1). When compared with MODIS-GPP, VPM-GPP showed higher

estimation in forests and grasslands but was lower in deserts (Fig.S4). Nevertheless, the variability of VPM-GPP agreed well with EC-derived GPP with an 8-day time interval and MODIS-GPP each year. Our

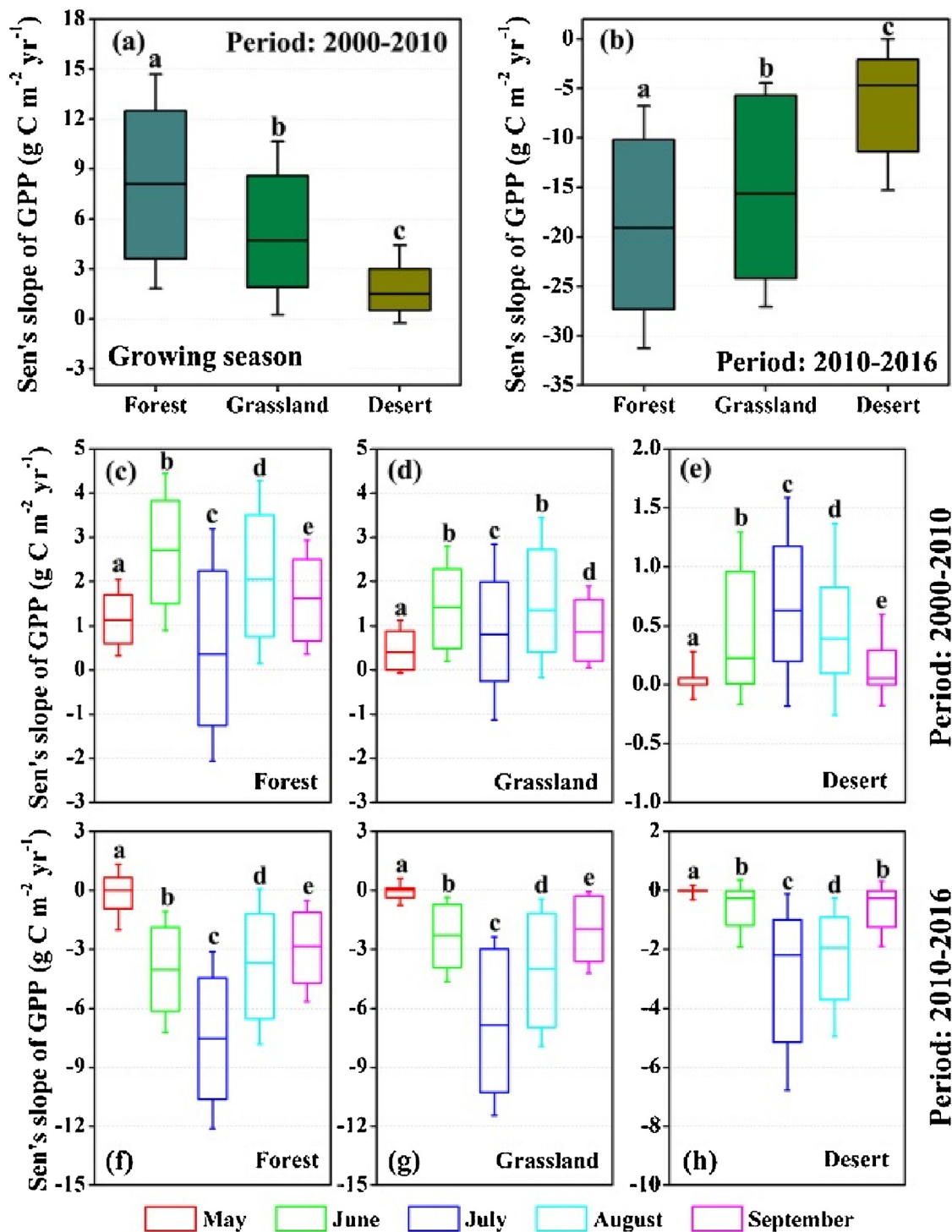


Fig. 6. The Sen's slope of GPP among biomes during the period of 2000–2010 and 2010–2016, respectively. Boxplot elements: box = values of 25th and 75th percentiles; horizontal line = median; whisker = \pm 1SD.

findings were in consistent with previous researches, showing that MODIS overestimated GPP at low productivity sites due to artificially high values of *f*APAR but underestimated GPP in the high productivity sites due to low values for LUE (Turner et al., 2006). Therefore, this study demonstrates that VPM-based GPP estimation is capable of tracking the seasonal variation of EC-GPP, and can be applied to monitor the interannual variation of GPP among biome types. The VPM is driven by the EVI, LSWI, PAR, temperature and maximum LUE. A few flux towers and limited meteorological stations are available in the QLMs. PAR is one of the primary sources of uncertainty in GPP

estimation (He et al., 2014). The noise due to cloud contamination in the satellite data and the different seasonality of EVI, especially during the leaf-expansion period, makes the EVI-GPP relationships complex (Nagai et al., 2010). EVI is strongly affected by diurnal and seasonal changes in solar elevation angle when vegetation is sparse (Sims et al., 2008). The maximum LUE depends on land cover types and is considered as a constant for a certain vegetation type. Much attention should be given to the variability of maximum LUE among vegetation types across a heterogeneous landscape (Wang et al., 2010). Moreover, the MODIS land cover type product at a 500 m spatial resolution

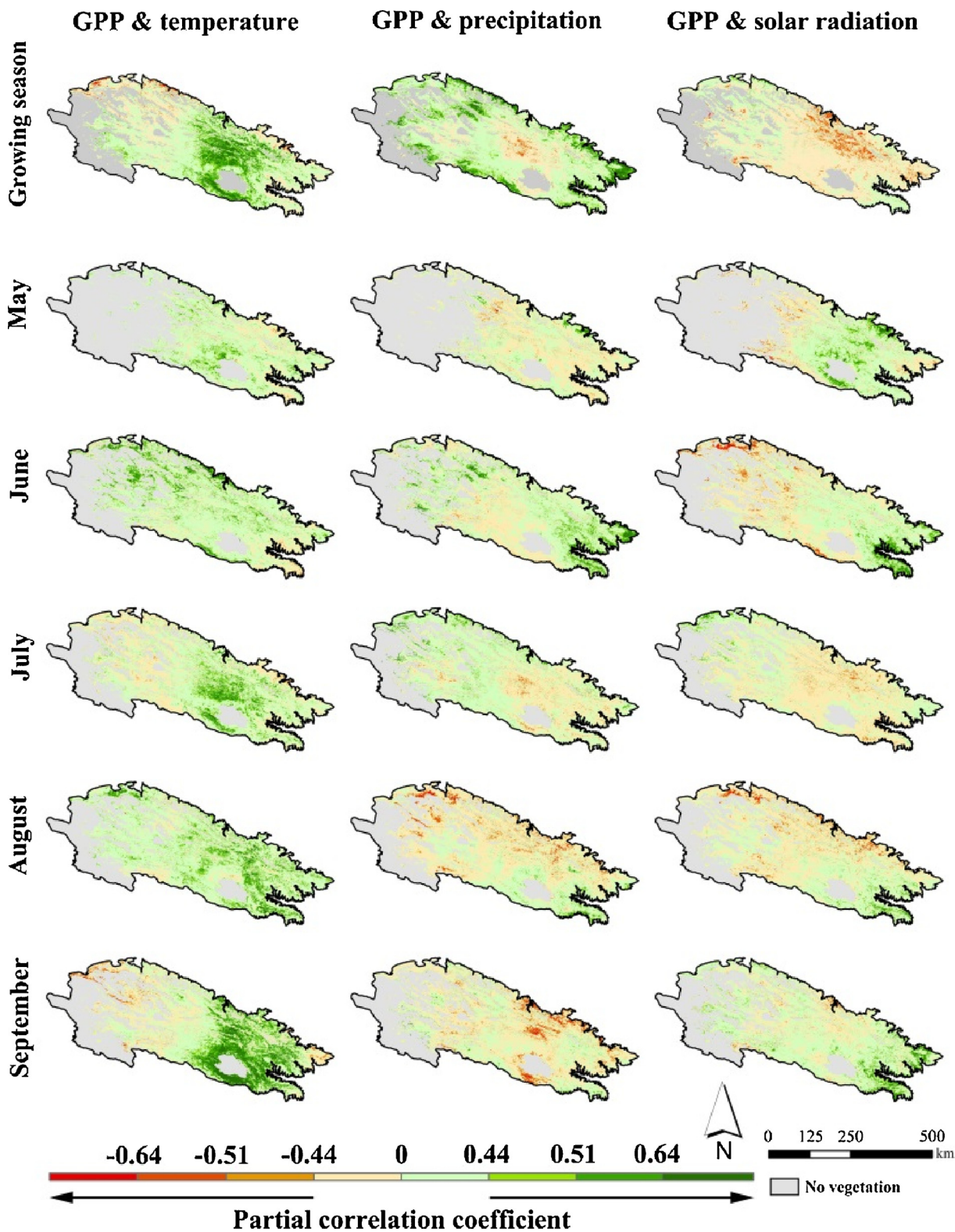


Fig. 7. The partial correlation coefficient of montly GPP with temperature, precipitation and solar radiation in each grid. The two arrows show the ranges that are significant.

contains a large number of mixed pixels, which reduces the accuracy of land cover classifications over the QLMs, characterized by heterogeneous and fragmented landscapes (Li et al., 2012). It is possible that the LSWI cannot fully characterize the impact of water availability on vegetation productivity (Yuan et al., 2015). All these errors will propagate in the VPM, reducing the accuracy of GPP estimation.

It should be noted that the distribution patterns of annual GPP were dependent on annual mean temperature and precipitation over the QLMs (Fig. 3). The decrease of GPP with rising temperature was induced by the decrease of precipitation with lowering elevation. Similarly, the decrease of GPP with rising annual precipitation was caused by lowering temperature with increasing elevation. Rising temperature

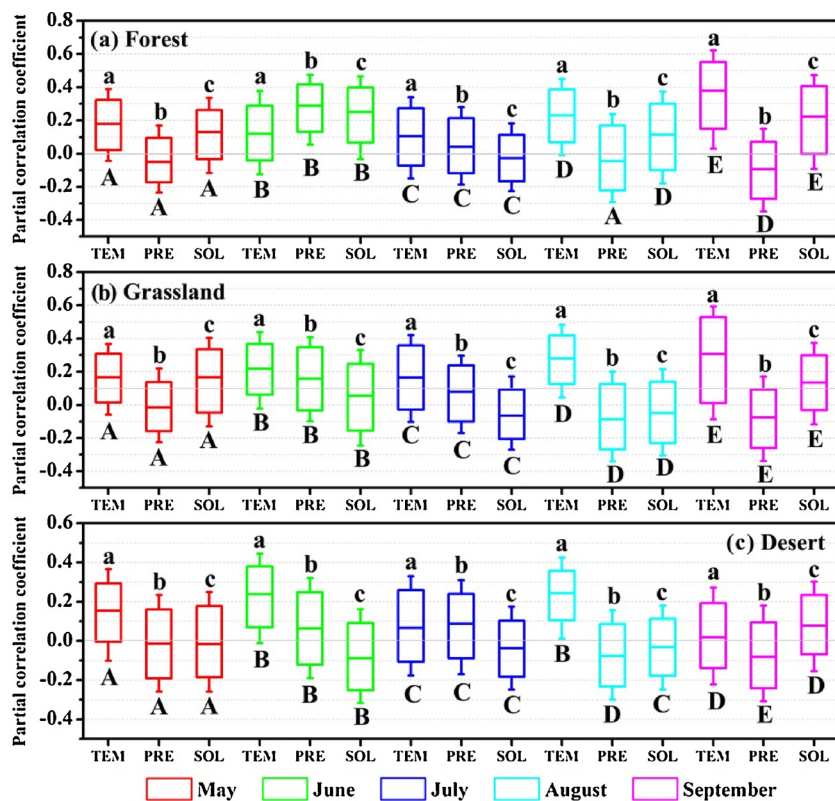


Fig. 8. The partial correlation coefficient of GPP with temperature (TEM), precipitation (PRE) and solar radiation (SOL) for different biomes at the monthly time scale. Different lower-case letters suggest significant differences among climate variables of the same month. Different capital letters show significant differences for different months of the same climatic factors.

leads to higher evaporative demand and reduced soil moisture (Cook et al., 2014). However, annual GPP decreased with annual precipitation when it was abundant but increased with rising temperature when it was low. At high altitudes, heat could outweigh moisture in allowing the establishment of vegetation community (Dawes et al., 2015). In this study, we first present the temperature and precipitation thresholds affecting the spatial distribution of annual GPP in the QLMs, having implications for simulating the spatial variability in GPP under future climate change.

4.3. Contrasting trends in GPP

We observed a significant increasing trend in growing season GPP in the QLMs for the period 2000–2010 (Fig. 4), and June, August and September contributed most to this trend in growing season GPP (Table S4). Our results were in consistent with previous studies, showing that the radial growth in trees and vegetation cover increased in the QLMs from 2000 to 2010 (Deng et al., 2013; Gao et al., 2018). However, there were clear decreases in growing season GPP in the QLMs for the period 2010–2016 (Fig. 4), and GPP reductions were dramatic across almost the whole area (Fig. 5), a finding that has not been reported before. The growing season mean NDVI and EVI decreased slightly (Fig. S5), suggesting decreased vegetation growth for this time period. July, August and September contributed most to this trend in growing season GPP (Table S4). We also found that higher-productivity biomes experienced higher changing rates in GPP than lower-productivity biomes (Fig. 6). Our findings highlight widespread GPP reductions at the middle and end of the growing season from 2010 to 2016. Special attention should be given to GPP as a key variable determining useful products and ecosystem services that may be at risk. Once multi-year calculated GPP data from EC flux towers under different climate zones and ecosystem types are available for the QLMs, analyses of EC-GPP will help reduce the uncertainty of VPM-GPP trends, improving our understanding of the carbon cycle of a dryland mountain ecosystem. Additionally, the length of the dataset analyzed (17 years), which is imposed by the availability

of MODIS imagery, represents a major constraint for the current investigation on abrupt changes of the GPP trend in the QLMs.

Previous studies have suggested that China has experienced warming hiatus since 1998, caused mainly by decreases in annual mean maximum temperature (Li et al., 2015). Likewise, we found that growing season mean temperature increased from 2000 to 2010 but decreased since 2010 (Fig. 4). Such contrasting trends also appeared in precipitation and solar radiation, coinciding with the trend in growing season GPP. Temperature, moisture and light conditions are the primary environmental controls on the CO₂ flux of Asian terrestrial ecosystems (Kato and Tang, 2008). In the central and southern parts, growing season GPP increased from 2000 to 2010 in response to rising temperature (Fig. 7), while a contrasting trend in growing season GPP from 2010 to 2016 was caused by decreased temperature (Fig.S6). The positive effect of rising temperature causing increased GPP was achieved by increasing photosynthetic capacity and prolonged growing season length (Nemani et al., 2003). In the western and eastern parts, precipitation primarily determined the trend in GPP (Fig. 7). The unique finding of this study was that variations in precipitation in June played a dominant role in the growing season GPP trend in the eastern portion of the QLMs, where most forests occurred. It highlights that the growth of evergreen coniferous forests is susceptible to drought, particularly at the beginning of the growing season, when the canopy leaf area is more responsive to water deficit (Croft et al., 2015). At the middle and end of the growing season, the seasonal GPP variation is more correlated with the canopy chlorophyll content, influenced primarily by the variability in leaf nitrogen contents and pigments (Dechant et al., 2017). The positive correlation between forest production and drought stress has been reported in our previous publications (Xu et al., 2016, 2018). We conclude that warming hiatus leads to declines in growing season GPP in the central and southern parts of the QLMs in 2010–2016. Drought results in GPP reductions in the western and eastern portions of the QLMs.

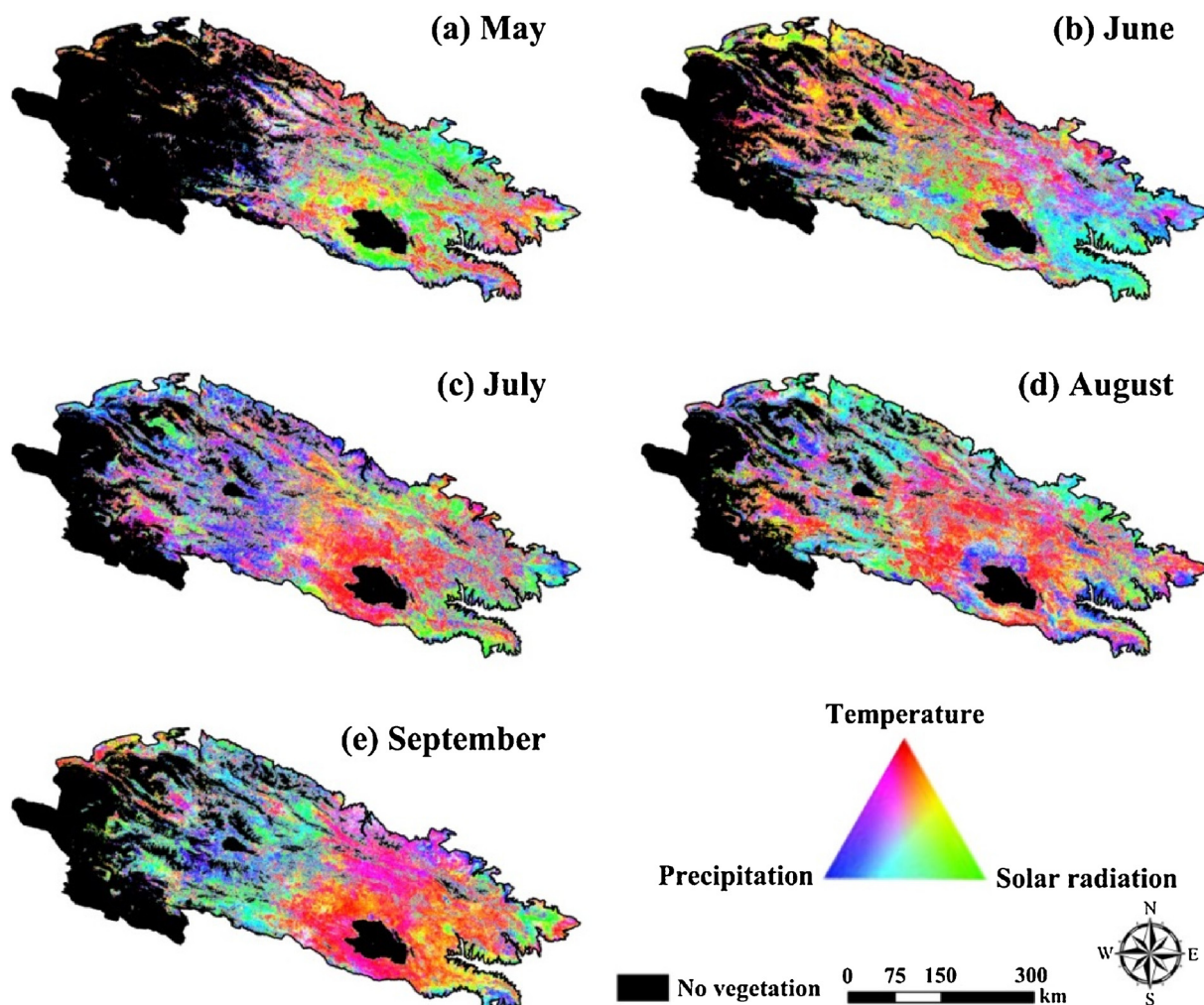


Fig. 9. The climate drivers for monthly GPP interannual variability.

4.4. The relationship between GPP and climate variables

The relationship between GPP and climate variables changed across seasons and biomes (Fig. 8). The positive effect of increased temperature was dominant in most vegetated regions in the growing season, mainly composed of evergreen coniferous forests, alpine meadows and alpine deserts. Rising temperature extends the range of growing season and promotes summer photosynthesis when moisture is nonlimiting (Jeong et al., 2011). The negative effect of rising temperature appeared in warm deserts and desert steppes (Fig. 7), where vegetation dynamics are controlled by moisture, and warming exacerbates plant water stress (Yao et al., 2016). The interannual variability in GPP was positively correlated with precipitation in June and July, when temperature and solar radiation were abundant. It was negatively related to precipitation in May, August and September, reflecting decreasing demand for soil moisture but increasing demand for temperature and light conditions, in line with previous studies (Zhang et al., 2008; Yan et al., 2016). Interestingly, our results identified a negative correlation between GPP and solar radiation in alpine deserts at the beginning and middle of the growing season (Fig. 8). A recent study suggests that enhanced UV radiation may slow photosynthesis and decrease plant biomass, but its effect is species-specific (Barnes et al., 2017). Overall, temperature and solar radiation accounted for most interannual variability in GPP for forests (Fig. 9). The reason is that Qinghai spruce is the dominant tree species, distributed mainly in the shady slope of the mountain. Temperature played a dominant role in the interannual variability in GPP

for most grasslands, mainly composed of alpine meadows, confirming earlier studies (Xu et al., 2017). In the western part, alpine deserts are the dominant ecosystem types, including primarily high elevation cushion-like and periglacial vegetation. Temperature became a stronger determinant of the variability in GPP at the beginning of the growing season, possibly because of its effect on germination and leaf green-up (He et al., 2018). On the other hand, precipitation followed by solar radiation primarily determined the GPP variability during the middle and end of the growing season, showing that even in high-altitude regions vegetation productivity responded to precipitation changes in a relatively arid environment. Understanding the seasonal variation of GPP to climatic factors among biomes is important for determining the climate controls of carbon fluxes in mountain ecosystems.

4.5. Research limitations

In the QLMs, the human-induced land cover changes are small. From 2000 to 2010, the forest area only increased 7 km². Croplands accounted for 0.7% of the total study area and are not included in the current research. The land cover transition between deserts and grasslands are significant but it is caused mainly by climate change, considering that alpine deserts are the major component of deserts and are distributed at high altitudes, where human activity is weak. In this study, the spatial resolution of GPP data is 500 m, and the effects from human activities on GPP variations may be reduced at landscape scales, since human activities play an important role in local regions, such as

mining and tourism. Results of the alpine desert are reported but the VPM is not validated. Considering that alpine deserts are mainly composed of C3 species, the VPM sets a constant maximum LUE (1.24 g C MJ^{-1}) for it. Future research needs to assess the performance of VPM in alpine deserts based on the field-based estimation of GPP derived from the EC method. Additionally, the downscaling of $0.5^\circ \text{CRU-NCEP}$ aims to match the temporal and spatial resolution of the MODIS record. The major challenge is to obtain raster layers of the VPM-GPP confined to the temporal record that matches with the EC-GPP dynamics rather than spatial resolutions. The accuracy of CRU-NCEP data and high frequency weather patterns that are not present in the downscaled data cause the uncertainty of simulated GPP with a temporal resolution of an 8-day.

5. Conclusions

The VPM has the potential to be used to examine the seasonal and interannual dynamics of GPP in mountainous regions, characterized by diverse ecosystems and complex terrain. To obtain meteorological data at high spatial resolutions under the circumstances of limited field observation, the Delta downscaling method performs well. Abrupt changes of the GPP trend in the QLMs were observed, due to variations in temperature and precipitation across regions. Widespread GPP reductions in recent years highlight special attention should be given to GPP as a key variable determining useful products and ecosystem services that may be at risk. We verified the hypothesis that the dependence of GPP on temperature was changed at different growth stages of various vegetation types over the QLMs. The effects of solar radiation were significant, at least in certain months in the QLMs. Temperature and solar radiation were the major drivers of forest GPP variability. Temperature was a critical determinant for grassland GPP variability. Moisture was more limiting than temperature and light for alpine desert GPP during the middle and end of the growing season. Long-term calculated GPP from the EC flux measurement is needed to reduce the uncertainty of VPM-GPP trends and its covariation with climate for future research.

Acknowledgements

This work was supported by the Fundamental Research Funds for the Central Universities (grant numbers lzujbky-2018-4) and the National Key Research and Development Program of China (grant numbers 2016YFE0203400). We thank anonymous referees for their comments that significantly improved this paper.

Appendix A. Supplementary data

Supplementary material related to this article can be found in the online version, at [doi:https://doi.org/10.1016/j.agrformet.2019.107628](https://doi.org/10.1016/j.agrformet.2019.107628).

References

Baldocchi, D.D., 2003. Assessing the eddy covariance technique for evaluating carbon dioxide exchange rates of ecosystems: past, present and future. *Glob. Change Biol.* 9, 479–492.

Barnes, P.W., Ryel, R.J., Flint, S.D., 2017. UV screening in native and non-native plant species in the tropical alpine: implications for climate change-driven migration of species to higher elevations. *Front. Plant Sci.* 8, 1451.

Beer, C., Reichstein, M., Tomelleri, E., Ciais, P., Jung, M., Carvalhais, N., Roedenbeck, C., Arain, M.A., Baldocchi, D., Bonan, G.B., Bondeau, A., Cescatti, A., Lasslop, G., Lindroth, A., Lomas, M., Luyssaert, S., Margolis, H., Oleson, K.W., Rouspard, O., Veenendaal, E., Viovy, N., Williams, C., Woodward, F.I., Papale, D., 2010. Terrestrial gross carbon dioxide uptake: global distribution and covariation with climate. *Science* 329, 834–838.

Cook, B.I., Smerdon, J.E., Seager, R., Coats, S., 2014. Global warming and 21st century drying. *Clim. Dyn.* 43, 2607–2627.

Croft, H., Chen, J.M., Froelich, N.J., Chen, B., Staebler, R.M., 2015. Seasonal controls of canopy chlorophyll content on forest carbon uptake: implications for GPP modeling.

J. Geophys. Res.-Biogeosci. 120, 1576–1586.

Dawes, M.A., Philipson, C.D., Fonti, P., Bebi, P., Haettenschwiler, S., Hagedorn, F., Rixen, C., 2015. Soil warming and CO₂ enrichment induce biomass shifts in alpine tree line vegetation. *Glob. Change Biol.* 21, 2005–2021.

Davi, H., Dufrene, E., Francois, C., Le Maire, G., Houstou, D., Bosc, A., Rambal, S., Granier, A., Moors, E., 2006. Sensitivity of water and carbon fluxes to climate changes from 1960 to 2100 in European forest ecosystems. *Agric. For. Meteorol.* 141, 35–56.

de Groot, R.S., Wilson, M.A., Boumans, R.M.J., 2002. A typology for the classification, description and valuation of ecosystem functions, goods and services. *Ecol. Econ.* 41, 393–408.

Dechant, B., Cuntz, M., Vohland, M., Schulz, E., Doktor, D., 2017. Estimation of photosynthesis traits from leaf reflectance spectra: correlation to nitrogen content as the dominant mechanism. *Remote Sens. Environ.* 196, 279–292.

Deng, S., Yang, T., Zeng, B., Zhu, X., Xu, H., 2013. Vegetation cover variation in the Qilian Mountains and its response to climate change in 2000–2011. *J. Mt. Sci.* 10, 1050–1062.

Diaz, H.F., Grosjean, M., Graumlich, L., 2003. Climate variability and change in high elevation regions: past, present and future. *Clim. Change* 59, 1–4.

Fang, S., He, Z., Du, J., Chen, L., Lin, P., Zhao, M., 2018. Carbon mass change and its drivers in a boreal coniferous forest in the Qilian Mountains, China from 1964 to 2013. *Forests* 9, 57.

Gao, L., Gou, X., Deng, Y., Wang, Z., Gu, F., Wang, F., 2018. Increased growth of Qinghai spruce in northwestern China during the recent warming hiatus. *Agric. For. Meteorol.* 260–261, 9–16.

He, Z., Du, J., Chen, L., Zhu, X., Lin, P., Zhao, M., Fang, S., 2018. Impacts of recent climate extremes on spring phenology in arid-mountain ecosystems in China. *Agric. For. Meteorol.* 260–261, 31–40.

He, H., Liu, M., Xiao, X., Ren, X., Zhang, L., Sun, X., Yang, Y., Li, Y., Zhao, L., Shi, P., Du, M., Ma, Y., Ma, M., Zhang, Y., Yu, G., 2014. Large-scale estimation and uncertainty analysis of gross primary production in Tibetan alpine grasslands. *J. Geophys. Res.-Biogeosci.* 119, 466–486.

Heimann, M., Reichstein, M., 2008. Terrestrial ecosystem carbon dynamics and climate feedbacks. *Nature* 451, 289–292.

Ichii, K., Hashimoto, H., Nemani, R., White, M., 2005. Modeling the interannual variability and trends in gross and net primary productivity of tropical forests from 1982 to 1999. *Glob. Planet. Change* 48, 274–286.

Jeong, S., Ho, C., Gim, H., Brown, M.E., 2011. Phenology shifts at start vs. end of growing season in temperate vegetation over the Northern Hemisphere for the period 1982–2008. *Glob. Change Biol.* 17, 2385–2399.

Jönsson, P., Klundh, L., 2004. TIMESAT—a program for analyzing time-series of satellite sensor data. *Comput. Geosci.* 30, 833–845.

Jia, X., Zha, T., Gong, J., Wang, B., Zhang, Y., Wu, B., Qin, S., Peltola, H., 2016. Carbon and water exchange over a temperate semi-arid shrubland during three years of contrasting precipitation and soil moisture patterns. *Agric. For. Meteorol.* 228, 120–129.

Jung, M., Reichstein, M., Bondeau, A., 2009. Towards global empirical upscaling of FLUXNET eddy covariance observations: validation of a model tree ensemble approach using a biosphere model. *Biogeosciences* 6, 2001–2013.

Jung, M., Vetter, M., Herold, M., Churkina, G., Reichstein, M., Zaehle, S., Ciais, P., Viovy, N., Bondeau, A., Chen, Y., Trusilova, K., Feser, F., Heimann, M., 2007. Uncertainties of modeling gross primary productivity over Europe: a systematic study on the effects of using different drivers and terrestrial biosphere models. *Glob. Biogeochem. Cycle* 21, GB4021.

Kato, T., Tang, Y., 2008. Spatial variability and major controlling factors of CO₂ sink strength in Asian terrestrial ecosystems: evidence from eddy covariance data. *Glob. Change Biol.* 14, 2333–2348.

Kruskal, W.H., Wallis, W.A., 1952. Use of ranks in one-criterion variance analysis. *J. Am. Stat. Assoc.* 47, 583–621.

Li, Q., Yang, S., Xu, W., Wang, X.L., Jones, P., Parker, D., Zhou, L., Feng, Y., Gao, Y., 2015. China experiencing the recent warming hiatus. *Geophys. Res. Lett.* 42, 889–898.

Li, S., Xiao, J., Xu, W., Yan, H., 2012. Modelling gross primary production in the Heihe river basin and uncertainty analysis. *Int. J. Remote Sens.* 33, 836–847.

Li, Z., Yu, G., Xiao, X., Li, Y., Zhao, X., Ren, C., Zhang, L., Fu, Y., 2007. Modeling gross primary production of alpine ecosystems in the Tibetan Plateau using MODIS images and climate data. *Remote Sens. Environ.* 107, 510–519.

Mann, H.B., 1945. Nonparametric tests against trend. *Econometrica* 13, 245–259.

Monteith, J.L., 1972. Solar radiation and production in tropical ecosystems. *J. Appl. Ecol.* 9, 747–766.

Mosier, T.M., Hill, D.F., Sharp, K.V., 2014. 30-Arcsecond monthly climate surfaces with global land coverage. *Int. J. Climatol.* 34, 2175–2188.

Nagai, S., Saigusa, N., Muraoka, H., Nasahara, K.N., 2010. What makes the satellite-based EVI-GPP relationship unclear in a deciduous broad-leaved forest? *Ecol. Res.* 25, 359–365.

Nakano, T., Nemoto, M., Shinoda, M., 2008. Environmental controls on photosynthetic production and ecosystem respiration in semi-arid grasslands of Mongolia. *Agric. For. Meteorol.* 148, 1456–1466.

Nemani, R.R., Keeling, C.D., Hashimoto, H., Jolly, W.M., Piper, S.C., Tucker, C.J., Myeni, R.B., Running, S.W., 2003. Climate-driven increases in global terrestrial net primary production from 1982 to 1999. *Science* 300, 1560–1563.

Nogués-Bravo, D., Araújo, M.B., Errea, M.P., Martínez-Rica, J.P., 2007. Exposure of global mountain systems to climate warming during the 21st century. *Glob. Environ. Change* 17, 420–428.

Sabretaftar, K., Mackey, B., Croke, B., 2011. Sensitivity of modelled gross primary productivity to topographic effects on surface radiation: a case study in the Cotter River Catchment, Australia. *Ecol. Model.* 222, 795–803.

Saigusa, N., Yamamoto, S., Hirata, R., Ohtani, Y., Ide, R., Asanuma, J., Gamou, M., Hirano,

- T., Kondo, H., Kosugi, Y., Li, S., Nakai, Y., Takagi, K., Tani, M., Wang, H., 2008. Temporal and spatial variations in the seasonal patterns of CO₂ flux in boreal, temperate, and tropical forests in East Asia. *Agric. For. Meteorol.* 148, 700–713.
- Sen, P.K., 1968. Estimates of the regression coefficient based on Kendall's tau. *J. Am. Stat. Assoc.* 63, 1379–1389.
- Sims, D.A., Rahman, A.F., Cordova, V.D., El-Masri, B.Z., Baldocchi, D.D., Bolstad, P.V., Flanagan, L.B., Goldstein, A.H., Hollinger, D.Y., Misson, L., Monson, R.K., Oechel, W.C., Schmid, H.P., Wofsy, S.C., Xu, L., 2008. A new model of gross primary productivity for North American ecosystems based solely on the enhanced vegetation index and land surface temperature from MODIS. *Remote Sens. Environ.* 112, 1633–1646.
- Sun, F., Lu, Y., Wang, J., Hu, J., Fu, B., 2015. Soil moisture dynamics of typical ecosystems in response to precipitation: a monitoring-based analysis of hydrological service in the Qilian Mountains. *Catena* 129, 63–75.
- Sun, M., Liu, S., Yao, X., Guo, W., Xu, J., 2018. Glacier changes in the Qilian Mountains in the past half-century: based on the revised first and second Chinese glacier inventory. *J. Geogr. Sci.* 28, 206–220.
- Turner, D.P., Ritts, W.D., Cohen, W.B., Gower, S.T., Running, S.W., Zhao, M., Costa, M.H., Kirschbaum, A.A., Ham, J.M., Saleska, S.R., Ahl, D.E., 2006. Evaluation of MODIS NPP and GPP products across multiple biomes. *Remote Sens. Environ.* 102, 282–292.
- Wagner, B., Liang, E., Li, X., Dulamsuren, C., Leuschner, C., Hauck, M., 2015. Carbon pools of semi-arid *Picea crassifolia* forests in the Qilian Mountains (north-eastern Tibetan Plateau). *Forest Ecol. Manag.* 343, 136–143.
- Wang, H., Jia, G., Fu, C., Feng, J., Zhao, T., Ma, Z., 2010. Deriving maximal light use efficiency from coordinated flux measurements and satellite data for regional gross primary production modeling. *Remote Sens. Environ.* 114, 2248–2258.
- Wang, X., Ma, M., Huang, G., Veroustraete, F., Zhang, Z., Song, Y., Tan, J., 2012. Vegetation primary production estimation at maize and alpine meadow over the Heihe River Basin, China. *Int. J. Appl. Earth Obs. Geoinf.* 17, 94–101.
- Wilby, R.L., Wigley, T., 1997. Downscaling general circulation model output: a review of methods and limitations. *Prog. Phys. Geog.* 21, 530–548.
- Wohlfahrt, G., Hammerle, A., Haslwanter, A., Bahn, M., Tappeiner, U., Cernusca, A., 2008. Seasonal and inter-annual variability of the net ecosystem CO₂ exchange of a temperate mountain grassland: effects of weather and management. *J. Geophys. Res.-Atmos.* 113, D08110.
- Xiao, X., Zhang, Q., Braswell, B., Urbanski, S., Boles, S., Wofsy, S., Moore, B., Ojima, D., 2004. Modeling gross primary production of temperate deciduous broadleaf forest using satellite images and climate data. *Remote Sens. Environ.* 91, 256–270.
- Williams, M., Rastetter, E.B., Fernandes, D.N., Goulden, M.L., Shaver, G.R., Johnson, L.C., 1997. Predicting gross primary productivity in terrestrial ecosystems. *Ecol. Appl.* 7, 882–894.
- Xu, H., Wang, X., Zhang, X., 2016. Decreased vegetation growth in response to summer drought in Central Asia from 2000 to 2012. *Int. J. Appl. Earth Obs. Geoinf.* 52, 390–402.
- Xu, H., Wang, X., Yang, T., 2017. Trend shifts in satellite-derived vegetation growth in Central Eurasia, 1982–2013. *Sci. Total Environ.* 579, 1658–1674.
- Xu, H., Wang, X., Zhao, C., Yang, X., 2018. Diverse responses of vegetation growth to meteorological drought across climate zones and land biomes in northern China from 1981 to 2014. *Agric. For. Meteorol.* 262, 1–13.
- Yan, M., Tian, X., Li, Z., Chen, E., Li, C., Fan, W., 2016. A long-term simulation of forest carbon fluxes over the Qilian Mountains. *Int. J. Appl. Earth Obs. Geoinf.* 52, 515–526.
- Yao, Y., Wang, X., Li, Y., Wang, T., Shen, M., Du, M., He, H., Li, Y., Luo, W., Ma, M., Ma, Y., Tang, Y., Wang, H., Zhang, X., Zhang, Y., Zhao, L., Zhou, G., Piao, S., 2018. Spatiotemporal pattern of gross primary productivity and its covariation with climate in China over the last thirty years. *Glob. Change Biol.* 24, 184–196.
- Yao, Z., Zhao, C., Yang, K., Liu, W., Li, Y., You, J., Xiao, J., 2016. Alpine grassland degradation in the Qilian Mountains, China—a case study in Damaying grassland. *Catena* 137, 494–500.
- Yuan, W., Cai, W., Nguy-Robertson, A.L., Fang, H., Suyker, A.E., Chen, Y., Dong, W., Liu, S., Zhang, H., 2015. Uncertainty in simulating gross primary production of cropland ecosystem from satellite-based models. *Agric. For. Meteorol.* 207, 48–57.
- Zhang, Y., Xiao, X., Wu, X., Zhou, S., Zhang, G., Qin, Y., Dong, J., 2017. Data descriptor: a global moderate resolution dataset of gross primary production of vegetation for 2000–2016. *Sci. Data* 4, 170165.
- Zhang, Y., Yu, Q., Jiang, J., Tang, Y., 2008. Calibration of Terra/MODIS gross primary production over an irrigated cropland on the North China Plain and an alpine meadow on the Tibetan Plateau. *Glob. Change Biol.* 14, 757–767.
- Zhao, C., Nan, Z., Cheng, G., 2005. Methods for modelling of temporal and spatial distribution of air temperature at landscape scale in the southern Qilian Mountains, China. *Ecol. Model.* 189, 209–220.
- Zhou, J., Cai, W., Qin, Y., Lai, L., Guan, T., Zhang, X., Jiang, L., Du, H., Yang, D., Cong, Z., Zheng, Y., 2016. Alpine vegetation phenology dynamic over 16 years and its covariation with climate in a semi-arid region of China. *Sci. Total Environ.* 572, 119–128.